ISSN (Print) 1226-1750
ISSN (Online) 2233-6656
Journal of Magnetics 22(3), 483-490 (2017) https://doi.org/10.4283/JMAG.2017.22.3.483

Integrated Calibration for the Cross Magnetic Gradiometer

Cheng Chi[1]*, Jun-Wei Lv[1], Dan Wang[2], Zhen-Tao Yu[2], and Jing-Li Huang[1]

[1]*Department of Control Engineering, Naval Aeronautical and Astronautical University, Yantai 264001, China*
[2]*Institute of Remote Sensing, Naval Submarine Academy, Qingdao 266001, China*

(Received 27 March 2017, Received in final form 7 July 2017, Accepted 7 July 2017)

The magnetic gradiometer onboard a maneuverable vehicle is subjected to not only magnetometer errors and misalignment errors but also magnetic interference of vehicle. Measurement precision of the magnetic gradiometer is greatly affected by those errors, so an integrated error calibration method is proposed in this paper. Firstly, considering vector magnetometer errors and magnetic interference, an integrated error calibration model for vector magnetometer is established, and ellipsoid fitting parameters are calculated by the least square algorithm under ellipsoid restriction, then the error calibration matrices are solved by the Cholesky factorization. Secondly, the misalignment error calibration matrices are obtained by solving the Orthogonal Procrustes problem. Finally, simulations and experiments with a cross magnetic gradiometer are performed to verify effectiveness and robustness of the proposed method. Results show that the proposed method can effectively calibrate the cross magnetic gradiometer, and measurement accuracy of the cross magnetic gradiometer is increased greatly.

Keywords : fluxgate magnetometer, magnetic interference, cross magnetic gradiometer, scalar calibration

1. Introduction

Magnetic gradient tensor detection [1, 2] is an effective detection method for the magnetic targets, such as unexploded ordnance, naval mines, submarines, or other magnetic objects. Many countries have developed their own magnetic gradiometer for magnetic targets detection, such as the hexahedron magnetic gradiometer designed by the Naval Surface Warfare Center, the tetrahedron magnetic gradiometer designed by the DSO National Laboratories, and so on.

The magnetic gradiometer is usually constructed of multiple vector magnetometers, such as superconducting quantum interference devices (SQUID) [3] or fluxgate magnetometers. Fluxgate magnetometer has many merits, such as low cost, small size and low power with relatively high sensitivity. However, the fluxgate magnetometer is subjected to bias, different scale factors and axis non-orthogonality [4], and different magnetometers have misalignment errors. Magnetic gradiometer has to be operated on a vehicle for magnetic targets detection. The magnetic gradiometer is also subjected to the magnetic interference of vehicle, including soft iron and hard iron interferences. The errors and vehicle magnetic interference have great influence on the measurement of the magnetic gradiometer, so the magnetic gradiometer must be calibrated before being used.

The vector magnetometer calibration methods are reported in many literatures, and they are divided into two kinds: vector calibration and scalar calibration. Vector calibration [5, 6] requires a 3D Helmholtz coil system to generate rigorous calibration field, and a high precision tri-axial non-magnetic platform to measure the attitude of the magnetometer. The calibration procedure is complicated and the calibration instruments are very expensive. However, in scalar calibration [7-10], it only needs to rotate the magnetometer under stable geomagnetic field environment. The calibration procedure is simple and easy to realize. Scalar calibration for the magnetic gradiometer generally consists of two steps: the first step is to calibrate the vector magnetometer errors and the second step is to calibrate the misalignment errors. Pang *et al*. [7], Yin *et al*. [8] and Gao *et al.* [9] have researched some scalar calibration methods for the magnetic gradiometer respectively. However, the vehicle magnetic interference has not been taken into consideration in these methods.

*Corresponding author: Tel: +86-13127072200
Fax: +86-0535-6635644, e-mail: cheng.chihhu@163.com

Yin *et al*. [10] have proposed an integrated calibration method for the cross magnetic gradiometer, in which vector magnetometer errors, misalignment errors, and vehicle magnetic interference are considered. However, a rotation of sensor output is introduced in the vector magnetometer calibration process, and a nonlinear method is proposed to calibrate the combined misalignment errors. Yu *et al.* [11, 12] have proposed some calibration methods for the tetrahedron magnetic gradiometer, in which the calibration parameters are solved by using the traceless and symmetric property of the magnetic gradient tensor. However the above methods have the following disadvantages: the convergence rates require further improvement, and the magnetic gradient tensor is traceless and symmetric, which is a necessary but not a sufficient condition for the magnetic gradiometer calibration.

In this paper, an integrated error calibration method of the cross magnetic gradiometer is proposed considering the vector magnetometer errors (scale factor, non-orthogonal error and bias), misalignment errors and the vehicle magnetic interference (soft iron interference and hard iron interference). Firstly, an integrated error calibration model for vector magnetometer is established, and ellipsoid fitting parameters are calculated by the least square algorithm under ellipsoid restriction, then the error calibration matrices of the vector magnetometer are given by the solution of the Cholesky factorization. Secondly, the Orthogonal Procrustes problem is used to calculate the misalignment error calibration matrices. Finally, simulations and experiments are carried out for verification of the integrated error calibration method.

2. The Cross Magnetic Gradiometer

2.1. The cross magnetic gradiometer

Magnetic gradient tensor is the vector gradient of the magnetic flux density $\boldsymbol{B}(B_x, B_y, B_z)$, which is defined as

$$\boldsymbol{G} = \nabla \boldsymbol{B} = \begin{bmatrix} \partial B_x/\partial x & \partial B_x/\partial y & \partial B_x/\partial z \\ \partial B_y/\partial x & \partial B_y/\partial y & \partial B_y/\partial z \\ \partial B_z/\partial x & \partial B_z/\partial y & \partial B_z/\partial z \end{bmatrix} = \begin{bmatrix} G_{11} & G_{12} & G_{13} \\ G_{21} & G_{22} & G_{23} \\ G_{31} & G_{32} & G_{33} \end{bmatrix}. \quad (1)$$

In an area which does not contain conduction currents, both the divergence and the curl of the magnetic flux density are zero, so the tensor is traceless and symmetric.

$$\nabla \cdot \boldsymbol{B} = \frac{\partial B_x}{\partial x} + \frac{\partial B_y}{\partial y} + \frac{\partial B_z}{\partial z} = 0,$$

$$\nabla \times \boldsymbol{B} = \begin{vmatrix} i & j & k \\ \dfrac{\partial}{\partial x} & \dfrac{\partial}{\partial y} & \dfrac{\partial}{\partial z} \\ B_x & B_y & B_z \end{vmatrix} = 0.$$

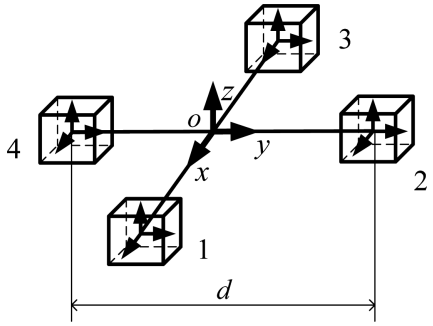

Fig. 1. The cross magnetic gradiometer.

In actual measurement application, the magnetic gradient tensor is approximated by the difference between two measurement readings of magnetic field at different locations. The magnetic gradiometer formed by fluxgate magnetometers has many different configurations, such as triangle, square, cross, tetrahedron, hexahedron and so on. The measurement accuracy of different configurations is analyzed in [13]. Simulation results show that the cross magnetic gradiometer has the highest measurement accuracy. Inspired by the above results, a cross magnetic gradiometer is designed in this paper, with the structure chart of the cross magnetic gradiometer shown in Fig. 1.

As shown in Fig. 1, the cross magnetic gradiometer consists of four fluxgate magnetometers (1 to 4). A right-handed coordinate system is established, the magnetometer 1 and the magnetometer 3 lie along x axes, the magnetometer 2 and the magnetometer 4 lie along y axes. The distance between two magnetometers along the same axes is d, and d is called the baseline distance of magnetic gradiometer. According to the difference equation, the magnetic gradient tensor of point o can be written as

$$\boldsymbol{G} = \frac{1}{d}\begin{bmatrix} B_{1x} - B_{3x} & B_{2x} - B_{4x} & B_{1z} - B_{3z} \\ B_{1y} - B_{3y} & B_{2y} - B_{4y} & B_{2z} - B_{4z} \\ B_{1z} - B_{3z} & B_{2z} - B_{4z} & B_{4y} - B_{2y} + B_{3x} - B_{1x} \end{bmatrix}, \quad (2)$$

where B_{1x} is the x component of the magnetic field measurement data of magnetometer 1. As shown in Eq. (2), vector magnetometer errors, misalignment errors and vehicle magnetic interference will influence the measurement precision directly, so the magnetic gradiometer must be calibrated before being used.

2.2. Integrated error calibration model for vector magnetometer

The magnetometer onboard a vehicle is subjected to non-orthogonal error, different scale factors, bias and vehicle magnetic interference. Non-orthogonal error is that the three axes of the triaxial fluxgate magnetometer

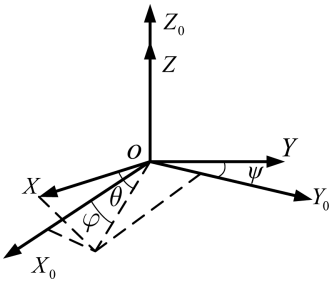

Fig. 2. Schematic diagram of the non-orthogonal error model.

may not be perfectly orthogonal. As shown in Fig. 2, suppose that $O-X_0Y_0Z_0$ is an ideal sensor's orthogonal coordinate system, and $O-XYZ$ is the actual coordinate system. Suppose that OZ is completely aligned with axis OZ_0. The plane YOZ is coplanar with the plane Y_0OZ_0. ψ denotes angle between the axis OY and OY_0. θ denotes angle between the axis OX and the plane X_0OY_0. φ denotes angle between the axis OX_0 and the projection of OX in the plane X_0OY_0.

Each axis of the magnetometer has different biases and sensitivities, so we suppose that $\boldsymbol{b}_o = \left[b_{ox}, b_{oy}, b_{oz}\right]^{\mathrm{T}}$ are the biases and s_x, s_y, s_z are the scale factors for OX, OY, OZ axes.

The magnetic interference sources of vehicle contain two main components: the soft iron effects and the hard iron bias. The soft iron effect is generated by the interaction of ferromagnetic material with an external magnetic field, and the soft iron interference changes the strength and direction of the external magnetic field. The hard iron bias stems from hard iron materials such as permanent magnets and electric cables carrying constant current. The hard iron bias, denoted as $\boldsymbol{B}_{HI} = [B_{HIx}, B_{HIy}, B_{HIz}]^{\mathrm{T}}$, is a constant magnetic field both in direction and strength, and it can be compensated with a simple constant.

Taking all these errors and interference sources into consideration, a mathematical model of magnetometer output is written as follows

$$\boldsymbol{B}_m = \boldsymbol{S}\boldsymbol{C}_{NO}(\boldsymbol{B} + \boldsymbol{B}_{SI} + \boldsymbol{B}_{HI}) + \boldsymbol{b}_o + \boldsymbol{\varepsilon}, \tag{3}$$

where $\boldsymbol{B}_m$, $\boldsymbol{B}$ are actual and theoretical outputs of the magnetometer respectively, $\boldsymbol{S} = \begin{bmatrix} k_x & 0 & 0 \\ 0 & k_y & 0 \\ 0 & 0 & k_z \end{bmatrix}$ is the scale factor matrix, $\boldsymbol{C}_{NO} = \begin{bmatrix} \cos\theta\cos\varphi & \cos\theta\sin\varphi & \sin\theta \\ 0 & \cos\psi & \sin\psi \\ 0 & 0 & 1 \end{bmatrix}$ is the non-orthogonal error coefficient matrix, $\boldsymbol{\varepsilon}$ is the measurement noise of magnetometer, $\boldsymbol{B}_{SI}$ is the soft iron interference, and it can be written as $\boldsymbol{B}_{SI} = \boldsymbol{K}\boldsymbol{B}$, where

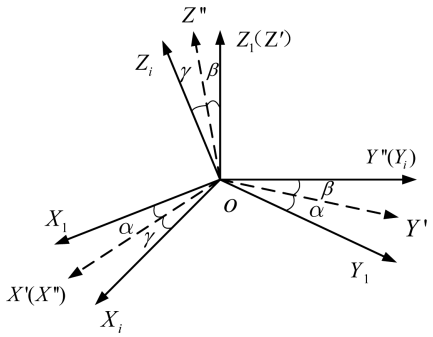

Fig. 3. Schematic diagram of misalignment error.

$\boldsymbol{K} = \begin{bmatrix} \alpha_{xx} & \alpha_{xy} & \alpha_{xz} \\ \alpha_{yx} & \alpha_{yy} & \alpha_{yz} \\ \alpha_{zx} & \alpha_{zy} & \alpha_{zz} \end{bmatrix}$ is the soft iron effect coefficient matrix, α_{ij} (i, j = x, y, z) are the proportional constants representing the constant relating the soft iron interference in the i direction resulting from the external magnetic field applied in the j direction. Eq. (3) is the integrated error calibration model of vector magnetometer.

2.3. Misalignment error model

Suppose that the magnetometer 1 is the reference magnetometer, and the $OX_1Y_1Z_1$ is the orthogonal coordinate system of the reference magnetometer. Suppose that $OX_iY_iZ_i$ is the orthogonal coordinate system of magnetometer i. Then rotate $OX_1Y_1Z_1$ to $OX_iY_iZ_i$ as follows: first, rotate $OX_1Y_1Z_1$ through angle α about Z_1 axes to $OX'Y'Z'$, then rotate $OX'Y'Z'$ through angle β about X' axes to $OX"Y"Z"$, at last, rotate $OX"Y"Z"$ through angle γ about Y'' axes to $OX_iY_iZ_i$.

As shown in Fig. 3, α, β, γ are misalignment angles. $\boldsymbol{B}_1 = \left[B_{1x}, B_{1y}, B_{1z}\right]^{\mathrm{T}}$ is the theoretical output of the reference magnetometer, and $\boldsymbol{B}_i = \left[B_{ix}, B_{iy}, B_{iz}\right]^{\mathrm{T}}$ is the theoretical output of magnetometer i. The mathematical relationship can be described as

$$\boldsymbol{B}_i = \boldsymbol{R}_1\boldsymbol{R}_2\boldsymbol{R}_3\boldsymbol{B}_1, \tag{4}$$

where $\boldsymbol{R}_1 = \begin{bmatrix} \cos\gamma & 0 & -\sin\gamma \\ 0 & 1 & 0 \\ \sin\gamma & 0 & \cos\gamma \end{bmatrix}$, $\boldsymbol{R}_2 = \begin{bmatrix} 1 & 0 & 0 \\ 0 & \cos\beta & \sin\beta \\ 0 & -\sin\beta & \cos\beta \end{bmatrix}$, $\boldsymbol{R}_3 = \begin{bmatrix} \cos\alpha & \sin\alpha & 0 \\ -\sin\alpha & \cos\alpha & 0 \\ 0 & 0 & 1 \end{bmatrix}$ are coordinate-transformation matrices. Eq. (4) is the misalignment error model.

3. Integrated Calibration for Cross Magnetic Gradiometer

3.1. Integrated error calibration for vector magnetometer

According to Eq. (3), the integrated error calibration model for vector magnetometer can be simplified as follows

$$\boldsymbol{B}_m = \boldsymbol{CB} + \boldsymbol{b} + \boldsymbol{\varepsilon}, \tag{5}$$

where $\boldsymbol{C} = \boldsymbol{SC}_{NO}(\boldsymbol{I} + \boldsymbol{K})$ is the combined error parameter matrix, $\boldsymbol{b} = \boldsymbol{SC}_{NO}\boldsymbol{B}_{HI} + \boldsymbol{b}_o$ is the combined bias matrix. Compared with the errors and the magnetic interference, the measurement noise is relatively small, and hence it is negligible, then the integrated error calibration model for vector magnetometer can be written as follows

$$\boldsymbol{B} = \boldsymbol{C}^{-1}(\boldsymbol{B}_m - \boldsymbol{b}). \tag{6}$$

According to Eq. (6), we know that the integrated calibration for vector magnetometer is to estimate the calibration matrices $\boldsymbol{C}^{-1}$ and $\boldsymbol{b}$, and then the actual output of the magnetometer can be calibrated to the theoretical output of the magnetometer. Within a homogeneous magnetic field, the intensity of the magnetic field is a constant. According to the integrated error calibration model in Eq.(6), we obtain

$$\boldsymbol{B}^{\mathrm{T}}\boldsymbol{B} = (\boldsymbol{B}_m - \boldsymbol{b})^{\mathrm{T}}(\boldsymbol{C}^{-1})^{\mathrm{T}}\boldsymbol{C}^{-1}(\boldsymbol{B}_m - \boldsymbol{b}) = \mathrm{const}. \tag{7}$$

Let $\boldsymbol{A} = (\boldsymbol{C}^{-1})^{\mathrm{T}}\boldsymbol{C}^{-1}$, then Eq. (7) can be simplified as follows

$$\boldsymbol{B}_m{}^{\mathrm{T}}\boldsymbol{A}\boldsymbol{B}_m - 2\boldsymbol{b}^{\mathrm{T}}\boldsymbol{A}\boldsymbol{B}_m + \boldsymbol{b}^{\mathrm{T}}\boldsymbol{A}\boldsymbol{b} - \boldsymbol{B}^{\mathrm{T}}\boldsymbol{B} = 0. \tag{8}$$

According to Eq. (8), we know that the locus of the theoretical output is a sphere, and the locus of the actual output is an ellipsoid, the general equation of an ellipsoid can be written as follows

$$\begin{aligned} &ax^2 + by^2 + cz^2 + 2fyz + 2gxz + 2hxy + 2px \\ &+2qy + 2rz + d = 0 \end{aligned}, \tag{9}$$

where $[x, y, z]^{\mathrm{T}}$ are actual outputs of the magnetometer. We can obtain the set of actual outputs $\{[x_i, y_i, z_i]^{\mathrm{T}}\}_{i=1}^{N}$ by presenting the magnetometer in different attitudes. Let the sensor output matrix $\boldsymbol{X}_i = [x_i^2, y_i^2, z_i^2, 2y_iz_i, 2x_iz_i, 2x_iy_i, 2x_i, 2y_i, 2z_i, 1]$ and the parameter matrix $\boldsymbol{P} = [a, b, c, f, g, h, p, q, r, d]^{\mathrm{T}}$, then the algebraic distance of the measurement point to the ellipsoid surface can be written as follows

$$\begin{aligned} F(\boldsymbol{X}_i, \boldsymbol{P}) = &ax_i^2 + by_i^2 + cz_i^2 + 2fy_iz_i + 2gx_iz_i \\ &+ 2hx_iy_i + 2px_i + 2qy_i + 2rz_i + d \end{aligned}. \tag{10}$$

The fitting can be approached by minimizing the sum of the algebraic distances,

$$\min \sum \left\| F(\boldsymbol{X}_i, \boldsymbol{P}) \right\| = \min \boldsymbol{P}^{\mathrm{T}}\boldsymbol{D}^{\mathrm{T}}\boldsymbol{D}\boldsymbol{P}, \tag{11}$$

where

$$\boldsymbol{D} = \begin{bmatrix} x_1^2 & y_1^2 & z_1^2 & 2y_1z_1 & 2x_1z_1 & 2x_1y_1 & 2x_1 & 2y_1 & 2z_1 & 1 \\ x_2^2 & y_2^2 & z_2^2 & 2y_2z_2 & 2x_2z_2 & 2x_2y_2 & 2x_2 & 2y_2 & 2z_2 & 1 \\ \vdots & \vdots & \vdots & \vdots & \vdots & \vdots & \vdots & \vdots & \vdots & \vdots \\ x_N^2 & y_N^2 & z_N^2 & 2y_Nz_N & 2x_Nz_N & 2x_Ny_N & 2x_N & 2y_N & 2z_N & 1 \end{bmatrix},$$

and then parameter matrix $\boldsymbol{P}$ can be solved by the least squares method. The parameter matrix $\boldsymbol{P}$ can be solved by the least squares method. The relationships between the parameter matrix $\boldsymbol{P}$ and calibration matrices $\boldsymbol{A}$, $\boldsymbol{b}$ are shown as follows

$$\boldsymbol{A} = \begin{bmatrix} a & h & g \\ h & b & f \\ g & f & c \end{bmatrix}, \tag{12}$$

$$\boldsymbol{b} = -\boldsymbol{A}^{-1}\begin{bmatrix} p \\ q \\ r \end{bmatrix}, \tag{13}$$

$$\boldsymbol{b}^{\mathrm{T}}\boldsymbol{A}\boldsymbol{b} - \boldsymbol{B}^{\mathrm{T}}\boldsymbol{B} = d. \tag{14}$$

Since the intensity of the magnetic field $\left\| \boldsymbol{B} \right\|$ is known, the calibration matrices $\boldsymbol{A}$, $\boldsymbol{b}$ can be calculated from Eq. (12), (13) and (14), and then the calibration matrix $\boldsymbol{C}^{-1}$ can be calculated from the decomposition of $\boldsymbol{A}$. In reference [10], an approximate value $\boldsymbol{Q}_E$ is obtained from singular value decomposition of $\boldsymbol{A}$

$$\boldsymbol{Q}_E = \boldsymbol{V}\sqrt{\boldsymbol{D}}\boldsymbol{V}^{\mathrm{T}}, \tag{15}$$

where $\boldsymbol{V}$ is a unitary matrix, and the columns of $\boldsymbol{V}$ are eigenvectors of $\boldsymbol{A}$. The non-zero elements of the diagonal matrix $\boldsymbol{D}$ is three eigenvalues of $\boldsymbol{A}$. We can come to the conclusion that $(\boldsymbol{Q}_E)^{\mathrm{T}}\boldsymbol{Q}_E = \boldsymbol{A}$. However, it is easy to see that any rotation matrix $\boldsymbol{R}_E$ satisfies $(\boldsymbol{R}_E)^{\mathrm{T}}\boldsymbol{R}_E = \boldsymbol{I}$ and $(\boldsymbol{R}_E\boldsymbol{Q}_E)^{\mathrm{T}}\boldsymbol{R}_E\boldsymbol{Q}_E = \boldsymbol{A}$, then a rotation of the sensor output will be introduced in the integrated error calibration procedure. Since $\boldsymbol{A}$ is a symmetric positive definite matrix, the Cholesky factorization of $\boldsymbol{A}$ is unique, and there is only one upper triangular matrix $\boldsymbol{C}^{-1}$ with strictly positive diagonal entries such that $(\boldsymbol{C}^{-1})^{\mathrm{T}}\boldsymbol{C}^{-1} = \boldsymbol{A}$, then the calibrated output of the magnetometer is in an ideal sensor's orthogonal coordinate system $O - X_0Y_0Z_0$ shown in Fig. 2. Then according to Eq. (6), we can calculate the calibrated outputs using $\boldsymbol{C}^{-1}$ and $\boldsymbol{b}$.

3.2. Misalignment error calibration

In the first step, the actual output of each magnetometer can be transformed into sensor's orthogonal coordinate system respectively. The calibrated output of each mag-

netometer will be identical if there is no misalignment error. However, If misalignment angles exist, there are rotation errors between calibrated output of magnetometer i and calibrated output of the reference magnetometer. According to the misalignment error model, the misalignment error calibration is converted to estimate the coordinate-transformation matrices. In this paper, a closed form solution for the misalignment error calibration is obtained by the solution of the Orthogonal Procrustes Problem. Suppose we get $N(N \geq 3)$ groups of measurement data by presenting the magnetic gradiometer in different attitudes. After the integrated error calibration for vector magnetometer, suppose $\boldsymbol{M}_i = [\boldsymbol{B}_{i1} \cdots \boldsymbol{B}_{iN}]$ is the calibrated output of magnetometer i, where $\boldsymbol{B}_{iN} = [B_{iNx}, B_{iNy}, B_{iNz}]^{\mathrm{T}}$, and $\boldsymbol{M}_1 = [\boldsymbol{B}_{11} \cdots \boldsymbol{B}_{1N}]$ is the calibrated output of the reference magnetometer. Assume that $\boldsymbol{M}_1\boldsymbol{M}_i^{\mathrm{T}}$ is nonsingular, and denote the corresponding singular value decomposition $\boldsymbol{M}_1\boldsymbol{M}_i^{\mathrm{T}} = \boldsymbol{U}\sum\boldsymbol{V}^{\mathrm{T}}$, where $\boldsymbol{U}$, $\boldsymbol{V}$ are unitary matrices, and Σ is a diagonal matrix. Then the optimal orthogonal matrix which most closely maps $\boldsymbol{M}_i$ to $\boldsymbol{M}_1$, Specifically,

$$\min_{\boldsymbol{R}} \sum_{j=1}^{N} \left\| \boldsymbol{B}_{1j} - \boldsymbol{R}\boldsymbol{B}_{ij} \right\|^2 \text{ subject to } \boldsymbol{R}^{\mathrm{T}}\boldsymbol{R} = \boldsymbol{I}. \quad (16)$$

The solution is unique and given by $\boldsymbol{R} = \boldsymbol{U}\boldsymbol{V}^{\mathrm{T}}$, then the output of magnetometer i can be transformed into orthogonal coordinate system of the reference magnetometer.

4. Simulations and Experiments

4.1. Simulations

The integrated calibration method is first analyzed using simulated data. The total intensity of the geomagnetic field is 50000nT, the declination angle is -7° and the inclination angle is 55°. Put the cross magnetic gradiometer under the stable geomagnetic field environment, and the sampling data is taken by presenting the cross magnetic gradiometer in different attitudes. The baseline distance is 0.5 m, and the error parameters of the four magnetometers are listed in Table 1.

Table 1. Error parameters of magnetometers.

	sensor 1	sensor 2	sensor 3	sensor 4
k_x	1.031	1.082	1.075	1.026
k_y	0.988	0.991	1.021	0.993
k_z	0.982	0.984	1.009	1.042
b_{ox}	75	−62	−33	65
b_{oy}	57	43	−49	51
b_{oz}	−42	39	47	−77
ψ	0.025	0.019	−0.014	0.011
φ	0.018	−0.013	0.027	0.016
θ	−0.023	0.021	0.017	−0.028
α	0	−0.029	0.032	−0.028
β	0	0.022	−0.026	−0.034
γ	0	0.024	0.033	0.038

In Table 1, unit of the bias is nT, and unit of the angle is rad. The soft iron effect coefficient matrix $\boldsymbol{K}$ and the hard iron bias $\boldsymbol{B}_{HI}$ of magnetometers are chosen as

$$\boldsymbol{K}_1 = \begin{bmatrix} 0.53 & 0.17 & 0.13 \\ 0.51 & 0.36 & 0.14 \\ -0.26 & 0.33 & 0.41 \end{bmatrix}, \quad \boldsymbol{K}_2 = \begin{bmatrix} 0.37 & -0.27 & 0.55 \\ 0.22 & 0.43 & -0.31 \\ 0.11 & 0.38 & 0.59 \end{bmatrix},$$

$$\boldsymbol{K}_3 = \begin{bmatrix} 0.12 & -0.07 & 0.19 \\ -0.17 & 0.58 & 0.22 \\ -0.21 & 0.11 & 0.13 \end{bmatrix}, \quad \boldsymbol{K}_4 = \begin{bmatrix} 0.39 & 0.18 & 0.37 \\ 0.14 & 0.46 & 0.23 \\ 0.23 & 0.17 & 0.52 \end{bmatrix},$$

$$\boldsymbol{B}_{HI1} = \begin{bmatrix} 1200 \\ -800 \\ 1400 \end{bmatrix} \text{nT}, \quad \boldsymbol{B}_{HI2} = \begin{bmatrix} -700 \\ 900 \\ 1100 \end{bmatrix} \text{nT},$$

$$\boldsymbol{B}_{HI3} = \begin{bmatrix} 1700 \\ 1200 \\ -300 \end{bmatrix} \text{nT}, \quad \boldsymbol{B}_{HI4} = \begin{bmatrix} 400 \\ -800 \\ 500 \end{bmatrix} \text{nT}.$$

The measurement noises in each axis of the four magnetometers are independent Gaussian white noises with mean of 0nT and variance of 9nT^2. 200 groups of measurement data are recorded. Error calibration matrices are calculated and shown in Table 2.

The actual outputs are calibrated using the error calibration matrices shown in Table 2, and the results are shown in Fig. 4 and Fig. 5. The total intensity of the geomagnetic field does not change with the misalignment error calibration procedure, so the total intensity of the geomagnetic field calibrated by the integrated calibration method for vector magnetometer is shown in Fig. 4. The fluctuations of the magnetic field intensity are large before calibration, but the calibrated outputs are closed to 50000nT. The RMS errors (root-mean-square errors) of the four magnetometers are 2.1734nT, 2.0735nT, 2.2402nT, 2.2659nT respectively, so we can come to the conclusion that the integrated calibration method for vector magnetometer can calibrate different scale factors error, non-orthogonal error, bias and magnetic interference of vehicle effectively. The actual outputs and the calibrated outputs of the magnetic gradient tensor components are shown in Fig. 5. After the integrated error calibration for the four magnetometers, the fluctuations of the magnetic gradient tensor components are still very large, then after the misalignment error calibration, the calibrated outputs are closed to 0nT/m.

Table 2. Error calibration matrices.

	C^{-1}	b	R
sensor 1	$\begin{bmatrix} 0.7217 & -0.4139 & 0.1580 \\ 0 & 0.7146 & -0.1526 \\ 0 & 0 & 0.6922 \end{bmatrix}$	$\begin{bmatrix} 1263.7 \\ -767.7 \\ 1333 \end{bmatrix}$	
sensor 2	$\begin{bmatrix} 0.6708 & 0.1036 & -0.2736 \\ 0 & 0.6824 & -0.0322 \\ 0 & 0 & 0.6203 \end{bmatrix}$	$\begin{bmatrix} -807.5 \\ 954.3 \\ 1120.5 \end{bmatrix}$	$\begin{bmatrix} 0.9335 & -0.252 & 0.255 \\ 0.2357 & 0.9673 & 0.0933 \\ -0.2702 & -0.027 & 0.9624 \end{bmatrix}$
sensor 3	$\begin{bmatrix} 0.8262 & 0.0663 & -0.0266 \\ 0 & 0.6301 & -0.2102 \\ 0 & 0 & 0.8584 \end{bmatrix}$	$\begin{bmatrix} 1823.1 \\ 1180 \\ -254.9 \end{bmatrix}$	$\begin{bmatrix} 0.8756 & -0.4786 & 0.0661 \\ 0.4829 & 0.8709 & -0.0917 \\ -0.0137 & 0.1122 & 0.9936 \end{bmatrix}$
sensor 4	$\begin{bmatrix} 0.7461 & -0.1265 & -0.2296 \\ 0 & 0.7054 & -0.1844 \\ 0 & 0 & 0.6205 \end{bmatrix}$	$\begin{bmatrix} 448.3 \\ -737.5 \\ 444.3 \end{bmatrix}$	$\begin{bmatrix} 0.8729 & -0.3251 & 0.3639 \\ 0.3233 & 0.9439 & 0.0677 \\ -0.3655 & 0.0585 & 0.929 \end{bmatrix}$

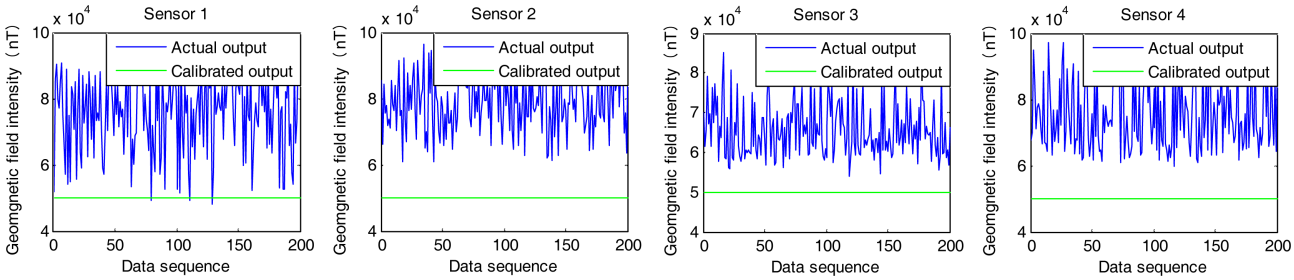

Fig. 4. (Color online) Comparison of geomagnetic field intensity before and after calibration.

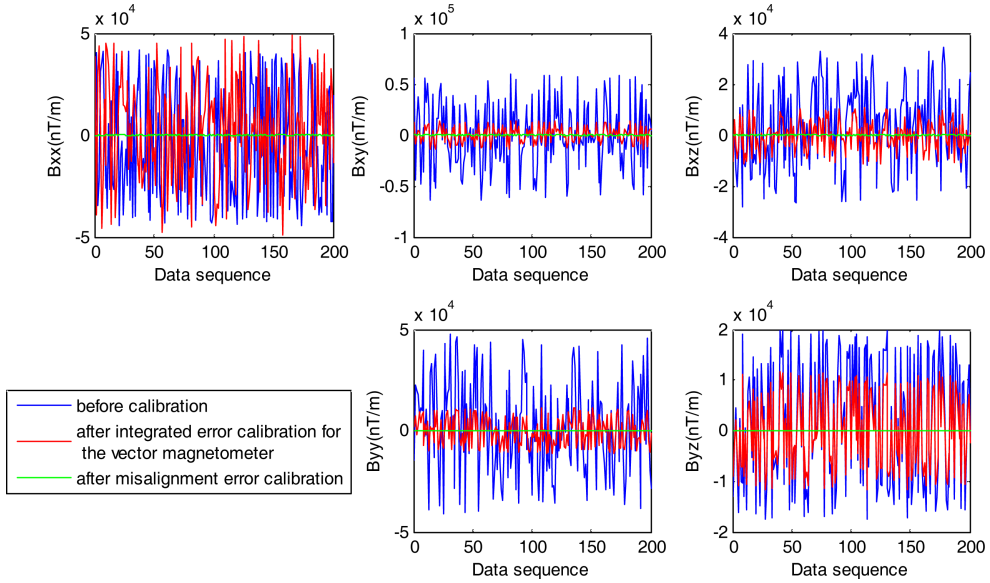

Fig. 5. (Color online) Comparison of magnetic gradient tensor components before and after calibration.

Table 3. RMS errors of magnetic gradient tensor components with different noises.

	Variance	B_{xx}	B_{xy}	B_{xz}	B_{yy}	B_{yz}
actual outputs	$9nT^2$	28438	31596	16136	22496	12278
calibrated outputs		6.4587	6.1209	6.0646	6.5588	6.1069
actual outputs	$12nT^2$	28438	31596	16136	22496	12278
calibrated outputs		7.35	7.1401	7.029	7.5727	7.0211
actual outputs	$15nT^2$	28439	31596	16136	22496	12278
calibrated outputs		8.2856	7.9134	7.9035	8.5516	7.8253

In order to verify the robustness of the proposed calibration method, three different simulations are carried out, the variances of the Gaussian white noises are set as $9nT^2$, $12nT^2$, $15nT^2$ respectively. RMS errors of magnetic gradient tensor components with different noises are shown in Table 3.

As the variance of the Gaussian white noises grow, the RMS errors will increase, and the RMS errors of calibrated outputs are less than 10nT/m, so the proposed calibration method has good accuracy and robustness.

4.2. Experiments

Experiments are carried out in Heikuang Mountain, Yantai, China. The cross magnetic gradiometer is shown in Fig. 6. Four fluxgate magnetometers are fixed on the aluminum frame with plastic bolts, and the baseline distance is 0.26m. A magnet is used to simulate the hard iron bias of the vehicle, and the magnet is with the size of 50 mm × 35 mm. A silicon steel sheet is used to simulate the soft iron effects. A proton magnetometer is used to monitor the ambient magnetic intensity, the resolution of the proton magnetometer is 0.1nT, the accuracy of the proton magnetometer is 1nT. Mean of the geomagnetic field intensity is 52561nT. 30 groups of measurement data are recorded by presenting the cross magnetic gradiometer in different attitudes.

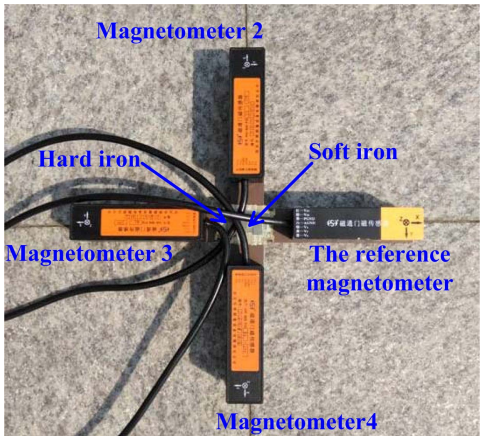

Fig. 6. (Color online) Cross magnetic gradiometer.

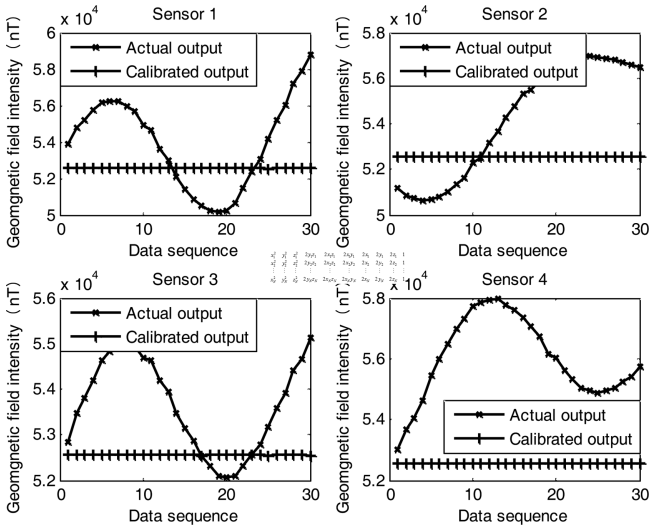

Fig. 7. Comparison of geomagnetic field intensity before and after calibration.

Comparison of geomagnetic field intensity before and after calibration is shown in Fig. 7. Before calibration, the fluctuations of the geomagnetic field intensity are large. However, after calibration, the calibrated outputs are closed to 52561nT. Comparisons of magnetic gradient tensor components before and after calibration are shown in Fig. 8. We know that the magnetic gradient tensor components should be 0nT/m in the uniform magnetic field. Because of the vector magnetometer errors, misalignment errors and magnetic interference of vehicle, the actual outputs of the magnetic gradient tensor components have big deviations. After calibration, the calibrated outputs are closed to 0nT/m.

Comparisons of RMS errors of magnetic gradient tensor components before and after calibration are shown in Table 4. The max RMS error of the magnetic gradient tensor components is 17109nT/m before calibration, and the max RMS error can be reduced to 35.8nT/m after calibration, so the proposed calibration method has good calibration accuracy. However, the geomagnetic field is not a uniform magnetic field, the gradient of the geomagnetic field is less than 0.02nT/m, and the ambient

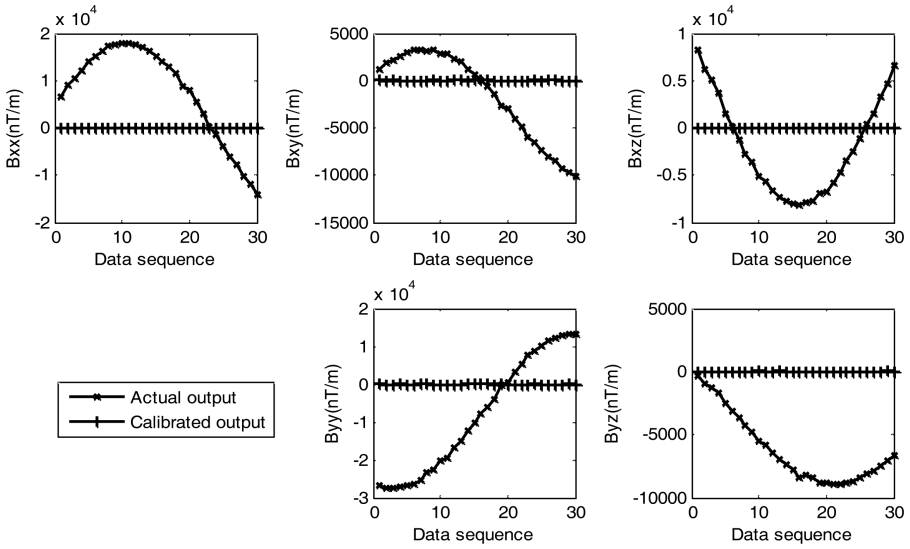

Fig. 8. Comparison of magnetic gradient tensor components before and after calibration.

Table 4. Comparison of RMS errors of magnetic gradient tensor components before and after calibration.

	B_{xx}	B_{xy}	B_{xz}	B_{yy}	B_{yz}
Actual output	12483	4833	5430	17109	6752
Calibrated output	32.9	35.8	29.4	27.5	25.2

magnetic field used for calibration is not perfect, so the RMS errors of the experiment results are larger than that of the simulation results.

5. Conclusion

Considering the vector magnetometer errors, misalignment errors and the magnetic interference of the vehicle, an integrated calibration method for the cross magnetic gradiometer is proposed. The simulation results show that: after calibration, the RMS errors of magnetic gradient tensor components with different noises are less than 10nT/m, so the proposed calibration method has good accuracy and robustness. The experiment results show that the max RMS error of the magnetic gradient tensor components is 17109nT/m before calibration, and the max RMS error can be reduced to 35.8nT/m after calibration, so the proposed integrated error calibration method can effectively calibrate the cross magnetic gradiometer. The proposed integrated error calibration method doesn't need the high precision tri-axial non-magnetic platform, and the calibration procedure only needs to be carried out under stable geomagnetic field environment. The calibration procedure is simple and convenient, so the proposed integrated error calibration method has high value for practical application.

Acknowledgement

This work was financially supported by the National High Technology Research and Development Program of China (Grant No. 2015AA0922).

References

[1] K. M. Lee and M. Li, IEEE Trans. Magn. **52**, 1 (2016).
[2] J. W. Lv, C. Chi, Z. T. Yu, B. Bi, and Q. S. Song, Acta Phys. Sin. **64**, 190701 (2015).
[3] P. Schmidt, D. Clark, K. Leslie, M. Bick, D. Tilbrook, and C. Foley, Explor. Geophys. **35**, 297 (2004).
[4] J. F. Vasconcelos, G. Elkaim, C. Silvestre, P. Oliveira, and B. Cardeira, IEEE Trans. Aerosp. Electron. Syst. **47**, 1293 (2011).
[5] H. F. Pang, M. C. Pan, C. B. Wan, J. F. Chen, X. J. Zhu, and F. L. Luo, IEEE Trans. Geosci. Remote Sens. **52**, 5670 (2014).
[6] J. Kuhlman, P. Collins, and T. Scarberry, Meas. Sci. Technol. **13**, 1124 (2002).
[7] H. F. Pang, S. T. Luo, Q. Zhang, J. Li, D. X. Chen, M. C. Pan, and F. L. Luo, Meas. Sci. Technol. **24**, 075102 (2013).
[8] G. Yin, Y. Zhang, H. Fan, G. Ren, and Z. Li, Sens. Actuators A Phys. **229**, 77 (2015).
[9] X. Gao, S. G. Yan, and B. Li, Chin. J. Sci. Instrum. **37**, 1226 (2016).
[10] G. Yin, Y. Zhang, H. Fan, G. Ren, and Z. Li, J. Magn. Magn. Mater. **374**, 289 (2015).
[11] Z. T. Yu, J. W. Lü, B. Bi, and J. Zhou, Acta Phys. Sin. **63**, 110702 (2014).
[12] J. Lv, Z. Yu, J. Huang, and J. Zhou, Adv. Math. Phys. **2013**, 1185 (2013).
[13] L. M. Liu, M.Sc. Dissertation, Jilin University, Changchun (2012).